Assessment of transition-metal coordination in glasses by electron energy-loss spectroscopy

Thomas Höche

Leibniz-Institut für Oberflächenmodifizierung e.V., Permoser Straße 15, D-04318 Leipzig, Germany

Michael Grodzicki

Institute of Mineralogy, University of Salzburg, Hellbrunner Straße 34, A-5020 Salzburg, Austria

Frank Heyroth

Interdisziplinäres Zentrum für Materialwissenschaften, Martin-Luther-Universität, Hoher Weg 8, D-06120 Halle a.d. Saale, Germany

Peter A. van Aken

Institut für Angewandte Geowissenschaften, Technische Universität Darmstadt, Schnittspahnstraße 9, D-64287 Darmstadt, Germany

In a combined experimental and theoretical study, it is shown that electronic structure calculations in the local density approximation on adequately sized model clusters unequivocally explain the Ti-$L_{2,3}$ electron energy-loss near-edge structure (ELNES) of pentahedrally coordinated Ti^{4+} in the fresnoite framework structure-type compound $Ba_2TiSi_2O_8$. Based on an in-depth discussion of the electronic structure-ELNES relationship in crystalline matter, the highly resolved Ti-$L_{2,3}$ ELNES of amorphous $Ba_2TiSi_2O_8$ ($2BaO \cdot TiO_2$-$2SiO_2$ glass) is interpreted in terms of Ti^{4+} coordination in the glass. The results demonstrate that high-resolution ELNES spectroscopy is a promising and powerful technique for atomistic-structure studies of amorphous matter.

PACS number(s): 71.23.Cq, 61.43.−j, 79.20.Uv

The structure of glasses is, due to poor medium-range and lacking long-range order, far from being fully understood. Although in recent years, topological approaches have been substantially brought forward, e.g., by Hobbs,[1] the theoretical assessment or even a classification of various types of amorphous networks remains extremely difficult. The same is true on the experimental side since methods capable of assessing the network structure, in particular with respect to medium-range ordering, are scarce. Diffraction methods, for example, comprising standard tools for the solution of crystalline structures, can be used only to a rather limited degree for structural studies of amorphous matter (e.g., in the form of x-ray small-angle scattering). Consequently, materials science challenges of tomorrow, like the amorphous-matter counterpart of polymorphism, polyamorphism,[2] can hardly be studied.

Due the the rather limited information assessable by each of the available individual techniques, in-depth studies of the structure of amorphous matter can only be accomplished by combining as many experimental techniques as possible. We shall prove that besides, e.g., Brillouin light scattering,[3] ^{2}H-NMR,[4] and neutron and high-energy x-ray diffractometry,[5] electron energy-loss spectroscopy (EELS) can reasonably supplement existing experimental approaches to the structure of disordered matter. Moreover, EELS studies can be performed at nanometer or even subnanometer resolution.

In modern transmission electron microscopes (TEM), EELS can be utilized to detect valence state[6] and coordination[7] of transition metals. As paradigmatically shown for the crystalline TiO_2 polymorphs rutile and anatase, the Ti-$L_{2,3}$ as well as O-K electron energy-loss near-edge structure (ELNES) most sensitively probes the atomis-

tic arrangement in the first and second coordination sphere of the target ion.[8]

In the past, EELS has not been broadly applied to glasses for the study of valence and coordination of its constituting elements. The potential of ELNES spectroscopy, however, has been impressively demonstrated by Jiang, Qiu, and Spence, who proved long-range structural fluctuations in a $CaO \cdot Al_2O_3$-$2SiO_2$ glass,[9] and by Hohl *et al.*,[10] where the Si-K ELNES of amorphous SiO has been interpreted in terms of Si oxidation states of Si^{4+} and Si^0. According to glass theory, disorder in glasses mainly concerns medium-range and long-range order and the glass network is constituted from individual, relatively undistorted coordination polyhedra. In this contribution, we will prove that the coordination of Ti^{4+} in a barium silicate glass can be derived from ELNES spectra provided that sufficiently high spectral resolution is available.

A $Ba_2TiSi_2O_8$ single crystal was grown using the automated Czochralski pulling technique with radio-frequency induction heating in an iridium crucible under flowing argon. A glass of the chemical composition $2BaO \cdot TiO_2$-$2SiO_2$ was prepared by melting $BaCO_3$, TiO_2, and SiO_2 in a Pt crucible at 1550 °C in an inductively heated furnace. After melting for 2 h, another 2 h of stirring, and additional 1 h of soaking, the melt was splat cooled between two copper plates. The obtained glass was clear and colorless with no indication of a bluish tint indicative of the presence of Ti^{3+}. TEM foils were prepared from $2BaO \cdot TiO_2$-$2SiO_2$ glass and single-crystalline $Ba_2TiSi_2O_8$ by mechanical thinning followed by double-sided Ar^+ ion-beam etching at 2.5 kV acceleration voltage. Static charging of the foil was avoided by selective carbon coating using the CoatMaster kit.[11]

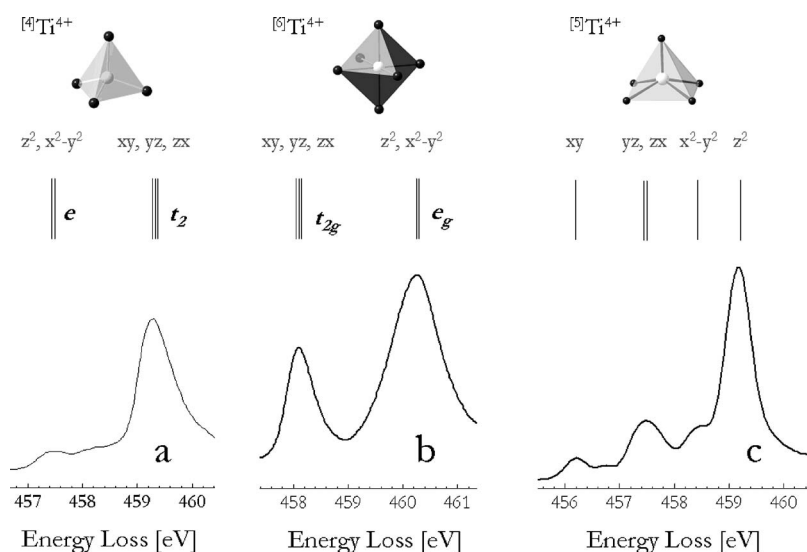TEM foils were examined by electron energy-loss spec-

FIG. 1. Energy schemes of $3d$ levels of Ti^{4+} ions in tetrahedral (β-Ba_2TiO_4), octahedral ($BaTiO_3$), and pentahedral ($Ba_2TiSi_2O_8$) coordination. In the lower part, corresponding Ti-L_3 ELNES features are plotted to scale to illustrate the relation between electronic structure and EELS data. Spectra a and b are taken from Brydson *et al.*[24]

troscopy using a dedicated scanning transmission electron microscope (VG HB501 UX) with a cold field emission gun and a parallel electron energy-loss spectrometer (Gatan Enfina 1000) attached. Routinely achieved energy resolution, defined as the full width at half maximum ΔE_{FWHM} of the zero-loss peak, amounts to $\Delta E_{FWHM} = 0.4$ eV, i.e., the spectral resolution at core-loss edges is on the order of 0.4–0.45 eV after averaging over approximately 20 spectra. EEL spectra were acquired at an illumination convergence semiangle of 14 mrad within a collection semiangle of 13 mrad. Radiation damage was minimized by spreading the beam over an area of about 50 nm (diameter) by defined defocusing of the objective lens. Approximately 20 spectra recorded at a dispersion of 0.05 eV/channel (each within 1 s) were energetically calibrated with subchannel relative accuracy and averaged after correcting for dark current and noise as well as for channel-to-channel gain variations of the detector. The background was subtracted using an inverse power-law function and multiple-scattering and tailing effects of the zero-loss peak were deconvoluted by the Fourier ratio technique using the corresponding low-loss and zero-loss spectra, acquired consecutively to core-loss spectra from the same specimen region.[12] As described in detail earlier,[7] absolute energy calibration is as precise as two channels (i.e., 0.1 eV for the present 0.05 eV dispersion).

The Ti-$L_{2,3}$ ELNES probes dipole-allowed excitations of electrons from occupied Ti($2p$) states into the narrow unoccupied conduction band with predominantly Ti($3d$) character and possibly some admixture from O($2p$) orbitals. Since for tetravalent Ti the $3d$ orbitals are empty, Ti^{4+} is ideally suited for an in-depth study of the coordination-dependent ELNES. In a tetrahedral or octahedral crystal-field, the d orbitals are split into two sublevels [Figs. 1(a) and 1(b)], whereas a four-fold splitting is observed for the square-pyramidal coordination occurring in the fresnoite framework structure-type compound $Ba_2TiSi_2O_8$ [Fig. 1(c)].

Since neither density functional theory nor multiple-scattering approaches can account for multiplet effects, the interpretation of the ELNES was supported by electronic structure calculations in the local density approximation

(LDA) on a series of model clusters with increasing size. The construction of these clusters starts from the experimentally determined crystal structure,[13] and follows the experience from previous cluster calculations on minerals,[7,14–16] Those calculations have shown that reliable results for spectroscopic data require that at least the surroundings of each oxygen atom of the first coordination sphere of the central ion have to be correctly described and that large negative cluster charges should be avoided. Accordingly, at least all cations of the second coordination sphere have to be included, comprising eight divalent barium and four (formally tetravalent) silicon atoms. Each of these cations is tenfold (Ba) or fourfold (Si) coordinated by oxygen atoms, leading to 53 oxygen atoms in the third coordination shell of Ti. Terminating the cluster at these oxygens gives, however, an inappropriate description of the electronic properties. First of all, the formal oxygen charge of −2 results in a large negative cluster charge that causes convergency problems if not compensated by a Madelung-type potential. Second, omitting the cations of the next shell bonded to the terminal oxygens produces unsaturated O($2p$) lone pairs that are in the same energy range as the Ti($3d$) orbitals and may occasionally also cause convergence problems. This stabilization can alternatively be attained by replacing some or all oxygens of the third coordination shell with fluorine atoms, or by adding further polyhedra, though at the expense of CPU time and memory space. Accordingly, the smallest reasonable cluster fulfilling these requirements has 39 atoms and the composition $[TiO_5\text{-}Si_4Ba_8O_4F_{17}]^{1+}$. This cluster is stepwise enlarged up to 16 atoms by replacing the fluorine atoms of the third shell by oxygens and adding at the same time the corresponding adjacent polyhedra until changes in the Ti($3d$) orbital energies are below 0.1 eV. The smallest, in this sense size-converged system, is a 142 atom cluster. The largest investigated cluster with 186 atoms has the composition $[TiO_5\text{-}(TiO)_2(Si_7Ti_2Ba_5O_{16}F_{14})_4]^{-2}$, contains 799 valence orbitals and comprises all the cations within a sphere of about 8 Å about the central Ti atom, and within a sphere of 6.7 Å all anions are correctly represented as oxygens.

The calculated Ti($3d$)-orbital energies for eight selected

TABLE I. Calculated Ti($3d$) orbital energies (in eV) in $Ba_2TiSi_2O_8$ with respect to d_{xy} and % $3d$ contribution (in brackets, $+4p_z$ in the last row) for eight differently sized clusters. The experimental positions of peak centers were determined by fitting one arctan function (reflecting the edge jump) and four Gaussians to the Ti-L_3 ELNES using the WinXAS code (Ref. 23).

Number of Atoms	d_{xy}	$d_{xz,yz}$	$d_{x^2-y^2}$	d_{z^2}
6	0(83)	0.67(75)	1.43(67)	2.23(72+3)
39	0(92)	1.41(73)	2.53(71)	3.39(68+9)
72	0(92)	1.37(74)	2.52(70)	3.35(68+8)
96	0(90)	1.23(74)	2.29(69)	3.24(68+7)
118	0(90)	1.18(75)	2.18(70)	3.21(69+6)
142	0(91)	1.33(74)	2.47(70)	3.37(69+8)
170	0(90)	1.28(75)	2.39(70)	3.32(69+7)
186	0(91)	1.29(75)	2.40(70)	3.34(69+7)
Experiment	0	1.3	2.3	3

clusters of different sizes are given in Table I, and the assignment of the d orbitals refers to a local coordinate system where the short, axial Ti-O_{ax} bond defines the z axis and the equatorial O_{eq} oxygen atoms are located on the x and y axes. It is obvious that the six-atom cluster $[TiO_5]^{6-}$ representing just the first coordination sphere does not yield meaningful results, though the splitting pattern is the same as for the size-converged clusters. The calculated ordering $d_{xy}, d_{xz,yz}, d_{x^2-y^2}, d_{z^2}$ of the Ti($3d$) orbitals is easily correlated with the structural features of the first coordination sphere. The (degenerate) $d_{xz,yz}$ orbitals undergo relatively strong π interaction with the $p_{x,y}$ orbitals of the short-bonded axial oxygen and are, accordingly, destabilized with respect to d_{xy}. The splitting of the antibonding σ orbitals of about 0.9 eV is about an order of magnitude larger than in the corresponding Ge-bearing fresnoite $Ba_2TiGe_2O_8$.[7] Additionally, the d_{z^2}-like molecular orbital contains some admixture from the Ti($4p_z$) orbital.

The occupation numbers of the Ti($3d$) orbitals are in accordance with this interpretation of the bonding modes. The weakly π-interacting d_{xy} is occupied with 0.17 electrons, the strongly π-interacting $d_{xz,yz}$ orbitals each with 0.46 electrons, and the σ-interacting $d_{x^2-y^2}$ and d_{z^2} orbitals each with 0.52 electrons. Further analysis of the charge distribution within the first coordination sphere of Ti yields $4s^{0.49}4p^{0.11}3d^{2.13}$ for the valence shell occupation of Ti. The resulting effective charge $Q_{eff}=1.27$ is considerably smaller than the formal charge or oxidation number of +4 and emphasizes the significant covalent interactions between the Ti($3d$) and the O($2p$) orbitals. Correspondingly, the effective charges of the oxygen atoms are far from the oxidation number of −2 (Table II). As expected, the overlap populations between Ti and O, i.e., the number of electrons n_{Ti-O} that can be assigned to a certain Ti-O bond, decrease with increasing distance (shown in the last column of Table II). The value for the short Ti-O_{ax} bond especially is rather large, whereas the populations of the equatorial bonds are in the typical range for bonds between oxygen and transition metals.[14–17] It is also seen in Table II that the ionicity of the Ti-O bonds increases with the bond distance, i.e., the oxygens become more negative while the overlap population decreases. At

this point, it shall be mentioned that with respect to ELNES features, the core-hole interaction becomes less important for large crystal-field splitting ("strong-field" case). Since in the present case the crystal-field splitting amounts ∼3 eV (between d_{xy} and d_{z^2}), core-hole interactions can be neglected in good approximation.

In excellent agreement with x-ray absorption near-edge structure data,[18] the experimental Ti-L_3 ELNES [corresponding to the Ti($2p^{3/2}$)→Ti($3d$) transition] of crystalline $Ba_2TiSi_2O_8$ possesses a characteristic fourfold splitting into peaks A_x (459.15 eV), B_x (457.5 eV), C_x (456.2 eV), and D_x (458.5 eV). Moreover, the energy positions of the peak centers are in almost quantitative agreement with the calculated orbital energy differences for the size-converged clusters with respect to the energetically lowest d_{xy} orbital (cf. Table I and Fig. 2): a deviation below 8% is well within the expected errors of the LDA yielding energies for the antibonding σ orbitals that usually are too large by up to 20%.

In addition to the $Ba_2TiSi_2O_8$ single-crystal, 2BaO-TiO_2-2SiO$_2$ glass has been investigated. The coordination of titanium in this glass has been determined earlier. From the Ti-K x-ray absorption near-edge structure, Farges[19] deduced the following coordination distribution for Ti^{4+}: 60±10% pentahedrally coordinated ($^{[5]}Ti^{4+}$), 20±10% octahedrally coordinated ($^{[6]}Ti^{4+}$), and another 20±10% tetrahedrally coordinated ($^{[4]}Ti^{4+}$). A similar coordination distribution (15% $^{[4]}Ti^{4+}$, 61% $^{[5]}Ti^{4+}$, 24% $^{[6]}Ti^{4+}$) was derived by Schneider *et al.*[20] from x-ray photoelectron spectroscopy (XPS) measurements.

In Fig. 2, the Ti-$L_{2,3}$ ELNES of crystalline $Ba_2TiSi_2O_8$ and 2BaO-TiO_2-2SiO$_2$ glass are juxtaposed and it is found that two sharp peaks (labeled A_G and B_G) and one shoulder (C_G) can be discerned in the Ti-L_3 ELNES of the glass. Such

TABLE II. Charge distribution within the first coordination sphere of Ti in $Ba_2TiSi_2O_8$ for the 186 atom cluster.

Atom	d_{Ti-O}[Å]	Q_{eff}	n_{Ti-O}
O_{ax}	1.698(11)	−0.554	0.739
O_{eq}	1.970(6)	−0.581	0.244
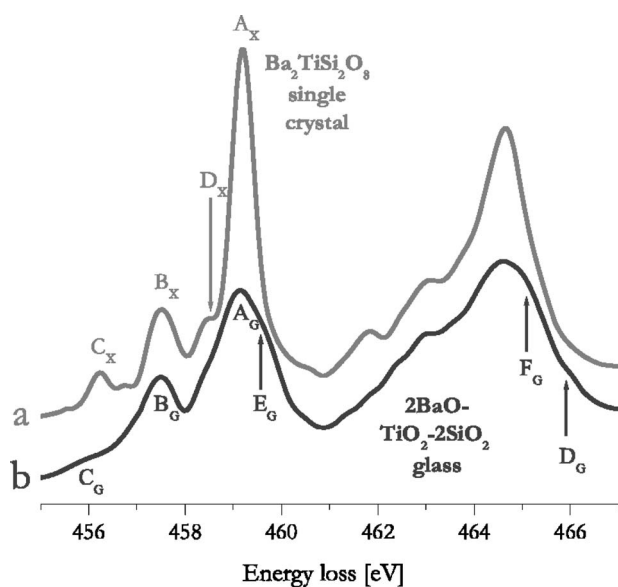
FIG. 2. Ti-$L_{2,3}$ ELNES of single-crystalline $Ba_2TiSi_2O_8$ and $2BaO \cdot TiO_2$-$2SiO_2$ glass. Both spectra have been normalized in the energy range between 455 eV and 467 eV and were vertically shifted for the sake of clarity.

relatively sharp peaks can only arise when the first coordination sphere (dominating the Ti-$L_{2,3}$ ELNES) is relatively well ordered. Nevertheless, the Ti-$L_{2,3}$ ELNES of the glassy samples is significantly broadened in comparison to the crystalline fresnoite Ti-$L_{2,3}$ ELNES, indicating that within the glass structure there is a certain range of bond lengths and bond angles contributing jointly to the near-edge structure.

From the peak positions (A_G, 459.15 eV; B_G, 457.5 eV), it is obvious that those dominant peaks correspond neither to $^{[4]}Ti^{4+}$ (e.g., β-Ba_2TiO_4 with peaks at 459.3 eV and 457.5 eV) nor $^{[6]}Ti^{4+}$ (like $BaTiO_3$ with peaks at 460.1 eV and 458.1 eV). Instead, the positions coincide with those of $^{[5]}Ti^{4+}$ in a regular pentahedral coordination, as found in crystalline $Ba_2TiSi_2O_8$ (A_x, 459.15 eV; B_x, 457.5 eV; C_x, 456.2 eV). According to recent molecular-orbital calculations,[7] peak $B_{G/X}$ sensitively reflects basal-plane distortions of TiO_5 square pyramids and would be shifted to lower energy losses for distorted TiO_5 pyramids. Although only vaguely apparent, the occurrence of feature C_G (at an energy loss of approximately 456 eV) further supports the interpretation that the coordination of titanium in $2BaO \cdot TiO_2$-$2SiO_2$ glass is dominated by a regular square-pyramidal arrangement of oxygen ions.

However, closer inspection of the $2BaO \cdot TiO_2$-$2SiO_2$ glass Ti-$L_{2,3}$ ELNES reveals some minor departures from the ideal symmetric peak shape and three further shoulders (not present in the Ti-$L_{2,3}$ ELNES of the single crystal) can be discerned at 466 eV (D_G), 459.6 eV (E_G), and 465.1 eV (F_G). Since the main t_2 peak of $^{[4]}Ti^{4+}$ is centered only 0.1 eV above the major peak of $^{[5]}Ti^{4+}$ (peak A_x in curve *a*, Fig. 2), those shoulders are most likely attributable to $^{[6]}Ti^{4+}$. Recalling Figs. 4 and 5 in Ref. 21, it is clear that more or less distorted TiO_6 octahedra (such as observed in anatase and rutile, respectively) can lead to significant changes in the relative intensities of the split e_g peaks. Considering these
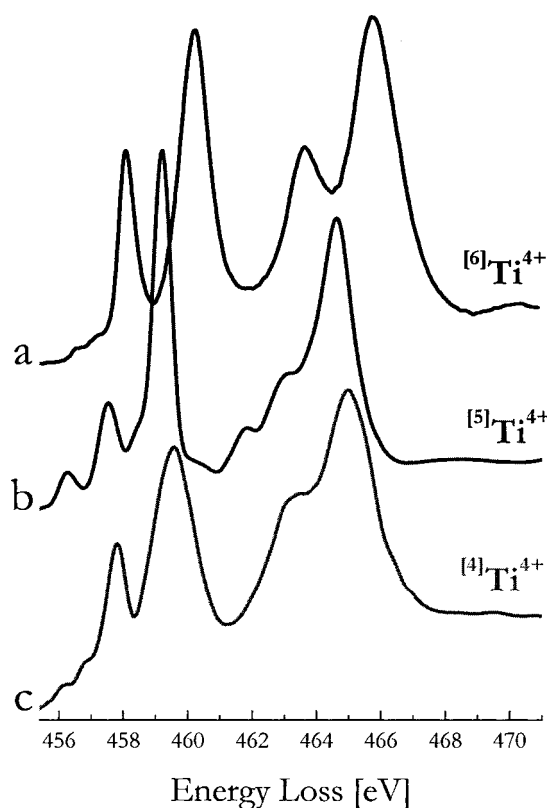

FIG. 3. Comparison of the Ti-$L_{2,3}$-ELNES for Ti in (a) tetrahedral coordination in β-Ba_2TiO_4: $^{[4]}Ti^{4+}$ (taken from Brydson *et al.*, Ref. 24); (b) fivefold (square-pyramidal) coordination found in fresnoite ($^{[5]}Ti^{4+}$); (c) octahedral coordination in $BaTiO_3$: $^{[6]}Ti^{4+}$ (taken from Brydson *et al.*, Ref. 24).

findings, it seems most likely that the minor $^{[6]}Ti^{4+}$ component in $2BaO \cdot TiO_2$-$2SiO_2$ glass is rather distorted (with apical oxygen-titanium-equatorial oxygen angles deviating from 90°). Due to peak overlap of the major features of pentahedrally and tetrahedrally coordinated Ti^{4+}, a possible (minor) amount of $^{[4]}Ti^{4+}$ cannot be detected, although the occurrence of peak D_G (at the Ti-L_2 ionisation edge) is indicative of the presence of tetrahedrally coordinated titanium; compare this to Fig. 3. Along the same line of argument, peak F_G is attributable to octahedrally coordinated Ti^{4+}, since as shown in Fig. 3, the main peak of $^{[6]}Ti^{4+}$ is located about 1.2 eV above the dominating peak of $^{[5]}Ti^{4+}$. It is, however, evident that $^{[6]}Ti^{4+}$ is not a major constituent of the $2BaO$—TiO_2-$2SiO_2$ glass structure. Our experimental Ti-$L_{2,3}$ ELNES is hence in broad agreement with earlier Ti-K x-ray absorption near-edge structure (XANES)[19] and XPS measurements.[20]

In summary, key findings presented here include (i) calculations of the electronic structure of titanium (using sufficiently large clusters) can be employed to reproduce and interpret experimental results of high-resolution EELS; (ii) the coordination of 3d transition metals in polyhedral glass networks (or, more general, amorphous matter) can be experimentally assessed by EELS in the transmission electron microscope, sufficiently high resolution provided. Hence, ELNES spectroscopy can be utilized to study the shape of polyhedra in disordered matter at very high spatial resolu-

tion. In next-generation transmission electron microscopes, a spectral resolution of 0.2 eV or better[22] and a minimum spot size below 5 Å will become available. With such instrumentation, spatially resolved coordination studies in glasses, amorphized crystals (e.g., by ion implantation), thin amorphous films, and nanometer-sized gate dielectrics in electronics devices will become feasible. The portfolio of experimental techniques used to study the structure of amorphous matter should therefore be extended by EELS in the TEM. In combination with other methods, the huge challenge to develop a better understanding of the atomistic structure of amorphous matter can be tackled.

[1] L. W. Hobbs, C. E. Jesurum, V. Pulim, and B. Berger, Philos. Mag. A **78**, 679 (1998).

[2] P. F. McMillan, M. Wilson, and M. C. Wilding, J. Phys.: Condens. Matter **15**, 6105 (2003).

[3] J. Kieffer, J. Non-Cryst. Solids **307**, 644 (2002).

[4] R. Lefort, A. Hedoux, Y. Guinet, E. Cochin, and M. Descamps, Eur. Phys. J. B **30**, 519 (2002).

[5] R. Weber, C. J. Benmore, J. Siewenie, J. Urquidi, and T. S. Key, Phys. Chem. Chem. Phys. **6**, 2480 (2004).

[6] T. Höche, P. Ohle, R. Keding, C. Rüssel, P. A. van Aken, R. Schneider, H. J. Kleebe, X. Q. Wang, A. J. Jacobson, and S. Stemmer, Philos. Mag. **83**, 165 (2003).

[7] T. Höche, P. A. van Aken, M. Grodzicki, F. Heyroth, R. Keding, and R. Uecker, Philos. Mag. **84**, 3117 (2004).

[8] R. Brydson, H. Sauer, W. Engel, J. M. Thomas, E. Zeitler, N. Kosugi, and H. Kuroda, J. Phys.: Condens. Matter **1**, 797 (1989).

[9] N. Jiang, J. Qiu, and J. C. H. Spence, Phys. Rev. B **66**, 054203 (2002).

[10] A. Hohl, T. Wieder, P. A. van Aken, T. E. Weirich, G. Denninger, M. Vidal, S. Oswald, C. Deneke, J. Mayer, and H. Fuess, J. Non-Cryst. Solids **320**, 255 (2003).

[11] The CoatMaster tool is available through 3D-Micromac AG (www.3d-micromac.com).

[12] P. A. van Aken and B. Liebscher, Phys. Chem. Miner. **29**, 188 (2002).

[13] S. A. Markgraf, A. Halliyal, A. S. Bhalla, and R. E. Newnham, Ferroelectrics **62**, 17 (1985).

[14] M. Grodzicki and G. Amthauer, Phys. Chem. Miner. **27**, 694 (2000).

[15] M. Grodzicki, S. Heuss-Assbichler, and G. Amthauer, Phys. Chem. Miner. **28**, 675 (2001).

[16] M. Grodzicki, G. J. Redhammer, G. Amthauer, V. Schünemann, A. X. Trautwein, B. Velickov, and P. Schmid-Beurmann, Am. Mineral. **88**, 481 (2003).

[17] A. Lougear, M. Grodzicki, C. Bertoldi, A. X. Trautwein, K. Steiner, and G. Amthauer, Phys. Chem. Miner. **27**, 258 (2000).

[18] G. S. Henderson, X. Liu, and M. E. Fleet, Phys. Chem. Miner. **29**, 32 (2002).

[19] F. Farges, J. Non-Cryst. Solids **244**, 25 (1999).

[20] M. Schneider, W. Richter, R. Keding, and C. Rüssel, J. Non-Cryst. Solids **226**, 273 (1998).

[21] R. Brydson, H. Sauer, W. Engel, J. M. Thomas, E. Zeitler, N. Kosugi, and H. Kuroda, J. Phys.: Condens. Matter **1**, 797 (1989).

[22] C. Mitterbauer, G. Kothleitner, W. Grogger, H. Zandbergen, B. Freitag, P. Tiemeijer, and F. Hofer, Ultramicroscopy **96**, 469 (2003).

[23] T. Ressler, J. Synchrotron Radiat. **5**, 118 (1998).

[24] R. Brydson, L. A. J. Garvie, A. J. Craven, H. Sauer, F. Hofer, and G. Cressey, J. Phys.: Condens. Matter **5**, 9379 (1993).